EPIGENETICS
2016, VOL. 11, NO. 4, 247–258
http://dx.doi.org/10.1080/15592294.2016.1148867

Taylor & Francis
Taylor & Francis Group

RESEARCH PAPER

Methylation profiling identified novel differentially methylated markers including *OPCML* and *FLRT2* in prostate cancer

Yu Wu[a], Jerry Davison[a], Xiaoyu Qu[a], Colm Morrissey[b], Barry Storer[a], Lisha Brown[b], Robert Vessella[b,c], Peter Nelson[a,b], and Min Fang[a,b]

[a]Fred Hutchinson Cancer Research Center, Seattle, WA; [b]University of Washington, Seattle, WA; [c]Puget Sound VA Health Care System, Seattle, WA

ABSTRACT

To develop new methods to distinguish indolent from aggressive prostate cancers (PCa), we utilized comprehensive high-throughput array-based relative methylation (CHARM) assay to identify differentially methylated regions (DMRs) throughout the genome, including both CpG island (CGI) and non-CGI regions in PCa patients based on Gleason grade. Initially, 26 samples, including 8 each of low [Gleason score (GS) 6] and high (GS $\geq$7) grade PCa samples and 10 matched normal prostate tissues, were analyzed as a discovery cohort. We identified 3,567 DMRs between normal and cancer tissues, and 913 DMRs distinguishing low from high-grade cancers. Most of these DMRs were located at CGI shores. The top 5 candidate DMRs from the low vs. high Gleason comparison, including *OPCML, ELAVL2, EXT1, IRX5*, and *FLRT2*, were validated by pyrosequencing using the discovery cohort. *OPCML* and *FLRT2* were further validated in an independent cohort consisting of 20 low-Gleason and 33 high-Gleason tissues. We then compared patients with biochemical recurrence (n=70) vs. those without (n=86) in a third cohort, and they showed no difference in methylation at these DMR loci. When GS 3+4 cases and GS 4+3 cases were compared, *OPCML*-DMR methylation showed a trend of lower methylation in the recurrence group (n=30) than in the no-recurrence (n=52) group. We conclude that whole-genome methylation profiling with CHARM revealed distinct patterns of differential DNA methylation between normal prostate and PCa tissues, as well as between different risk groups of PCa as defined by Gleason scores. A panel of selected DMRs may serve as novel surrogate biomarkers for Gleason score in PCa.

ARTICLE HISTORY
Received 9 October 2015
Revised 22 January 2016
Accepted 27 January 2016

KEYWORDS
DMR (differentially methylated regions); methylation profiling; prostate cancer

Introduction

Prostate cancer (PCa) is the most common cancer in men in the US. The natural history and clinical course of PCa is very heterogeneous: some are indolent with little effect on overall lifespan, whereas others can progress to lethal metastatic disease. The test commonly used to screen for PCa is the prostate specific antigen test (PSA); however, many other factors can affect PSA levels and result in high false-positive findings.[1] Furthermore, current therapeutic modalities have complications that may lead to significant morbidity.[2] Therefore, new methods are needed to distinguish indolent cancers from their aggressive counterparts.

One promising approach is DNA methylation profiling. Changes in DNA methylation, with accompanied epigenetic gene silencing, appear to be the earliest somatic genomic alterations recognized in human PCa and continue throughout disease progression.[3] Hypermethylation of promoter CpG islands (CGIs) can silence tumor suppressor genes early during tumorigenesis, while significant global hypomethylation arises later in PCa progression.[4-6] It is likely that different patterns of DNA methylation may distinguish aggressive vs. indolent PCa and predict responses to specific treatments. Earlier studies have shown that promoter hypermethylation of specific genes are associated with PCa progression. The best characterized gene, glutathione S-transferase-π (*GSTP1*), shows promoter hypermethylation in more than 90% of PCas from numerous independent analyses.[3] Other methylation-mediated gene silencing has been reported in more than 40 genes, including *APC, RARβ*, and *RASSF1A*, and the number continues to grow.[7-9] However, no consistent conclusions can be drawn regarding the predictive value of these methylation markers.

In addition, most studies that evaluate global gene methylation focus on the promoter CGI region and leave the regions outside CGIs largely unexplored. However, recent studies have demonstrated that methylation of CpG dinucleotides up to 2 kb away from CGI (the CGI "shores") can better distinguish different tissues as well as cancer and normal tissues.[10,11] We applied the comprehensive high-throughput arrays for relative methylation method (CHARM), which is a custom-designed NimbleGen HD2 microarray containing approximately 4.6 million CpG sites across the genome, to thoroughly examine all CpG dinucleotides in the genome. Because CHARM includes all CpGs in the genome, it is a non-biased methylation array that allows the identification of differentially methylated regions (DMRs) located in both CGI and non-CGI regions. We have successfully identified a series of genome-wide DMRs that

CONTACT Min Fang mfang@fhcrc.org
Supplemental data for this article can be accessed on the publisher's website.

can stratify normal vs. PCa and low-grade vs. high-grade PCa cases based on the Gleason score.

Results

CHARM effectively identified methylation differences between normal vs. prostate cancer and low Gleason vs. high Gleason cases

The CHARM assay was performed using 10 normal prostate tissues, 8 low Gleason score (GS) and 8 high Gleason score PCa samples (Table 1). All probes were displayed in the scatter plot with a subset of probes grouped into significant DMRs ($P<0.01$, highlighted in red) (Fig. 1A), with 7% of the total probes constituting significant DMRs in the comparison of normal vs. cancer, and 2% in low Gleason vs. high Gleason. There were 2,101 hypermethylated and 1,456 hypomethylated DMRs in the PCa samples compared with normal samples (Fig. 1B, C). In addition, we observed a total of 913 DMRs showing differential methylation between low Gleason and high Gleason samples, with 613 hypermethylated DMRs and 300 hypomethylated DMRs in high Gleason samples (Fig. 1B, C). There were 666 regions overlapping the DMR groups of normal vs. cancer (18.6% of total DMRs) and low vs. high Gleason samples (72.9% of total DMRs) (Fig. 1D).

To analyze the functional enrichment of the genes related to methylation changes, we performed integrative functional analysis using Ingenuity Pathway Analysis (IPA) (Table 3). In normal vs. PCa, the top network includes RNA posttranscriptional modification, cell cycle and cellular assembly, and organization networks. The top 3 bio-functions related to diseases and disorders are developmental disorder, skeletal and muscular disorders, and cancer. The top canonical pathway is the EIF2 signaling pathway. Regarding low vs. high Gleason cases, the top network involves embryonic development, nervous system development and function, and organ development. Similar to the results of normal vs. PCa, the top bio-function related to diseases is developmental disorder. The top canonical pathway is basal cell carcinoma signaling.

Table 1. Clinical pathological characteristics of the patients of discovery and validation cohort.

	Discovery cohort		Validation cohort	
	Low Gleason (GS=6) N=8	High Gleason (GS≥7) N=8	Low Gleason (GS=6) N=20	High Gleason (GS≥7) N=33
Gleason Score				
6 (3+3)	20	0	8	0
7 (3+4)	0	0	0	0
7 (4+3)	0	6	0	19
8-9	0	2	0	14
Age (y) at time of RRP*				
mean ± SD	61±1	61±2	54±6	62±8
Range	59-62	59-63	44-70	45-76
Race				
Caucasian	7	7	18	28
Asian	0	0	0	2
Black	0	1	0	1
Unknown	1	0	2	2
PSA at diagnosis, ng/ml				
≤10	7	4	18	15
>10	1	4	2	18
mean ± SD	6.0±2.1	14.3±14.2	7.6±5.8	17.2±18.0
Pathological stage				
T2	5	1	16	3
T3	3	7	4	30
Surgical margin status				
Negative	4	4	16	16
Positive	3	4	4	17
Abuts	1	0	0	0
Extra capsular extension				
Negative	5	2	2	10
Positive	3	6	18	23

*The mean age of patients who provided adjacent normal samples (N=10) were 61±1 years (range, 59 to 63 years). Among these, 8 are Caucasians; one is black; and the race of the remaining one is unknown.

Most DMRs are located at CGI shores

We next determined the distribution of the identified DMRs in the genome in relation to CGIs. If DMRs are distributed according to CpG density, the simulated frequency of DMR locations across the genome should follow the pattern shown as the white bars in Fig. 2 (the null hypothesis). However, our data demonstrated the distribution pattern of CHARM-identified DMRs to be as shown by the black bars. In both, the comparison of low vs. high Gleason grade (Fig. 2A) and the comparison of normal vs. PCa samples (Fig. 2B), significantly more DMRs were located within 2 kb of CGIs (i.e., on the "shore") rather than within CGIs. In the comparison of normal vs. PCa, only 17.7% of the DMRs were in CGIs, compared to 68.2% in shores; an additional 14.1% of the DMRs were located greater than 2 kb away from CGIs. Similarly, in the comparison of low vs. high Gleason cases, the percentage of DMRs located in CGIs, shores and beyond was 21.1%, 59.5%, and 19.4%, respectively. The most enriched genomic regions for DMRs in both cases were 0-500 bp away from CGIs, with 31.3% in normal vs. PCa and 26.2% in low vs. high Gleason.

A panel of DMRs is validated using pyrosequencing

The top 10 DMRs ranked by nominal *P*-values based on the CHARM statistics in both comparisons are listed in Supplemental Table 2, with their location relative to the nearest genes and CGIs, and the methylation status. For DMRs located in untranslated regions (UTRs) or areas away from genes, the genes located nearest to the DMR were used for their names. Aiming to identify differential DNA methylation to distinguish high-risk from low-risk PCa, 6 top candidate DMRs selected from the low vs. high Gleason result list, which allowed for successful design and performance of the pyrosequencing assay, were tested using quantitative methylation pyrosequencing analysis to confirm the CHARM result. The panel of 6 DMRs included *OPCML, ELAVL2, EXT1, IRX5, FLRT2*, and *MAB21L1*. We analyzed 4 types of different comparisons for each DMR in the panel: 1) normal vs. low Gleason, 2) normal vs. high Gleason, 3) normal vs. PCa, and 4) low vs. high Gleason. All six DMRs were differentially methylated in normal vs. high Gleason ($P<0.01$) and normal vs. PCa ($P\leq0.01$). For the comparison of normal vs. low Gleason, all except *OPCML* showed differential methylation patterns ($P<0.05$). For the comparison of low vs. high Gleason, *OPCML, ELAVL2,*

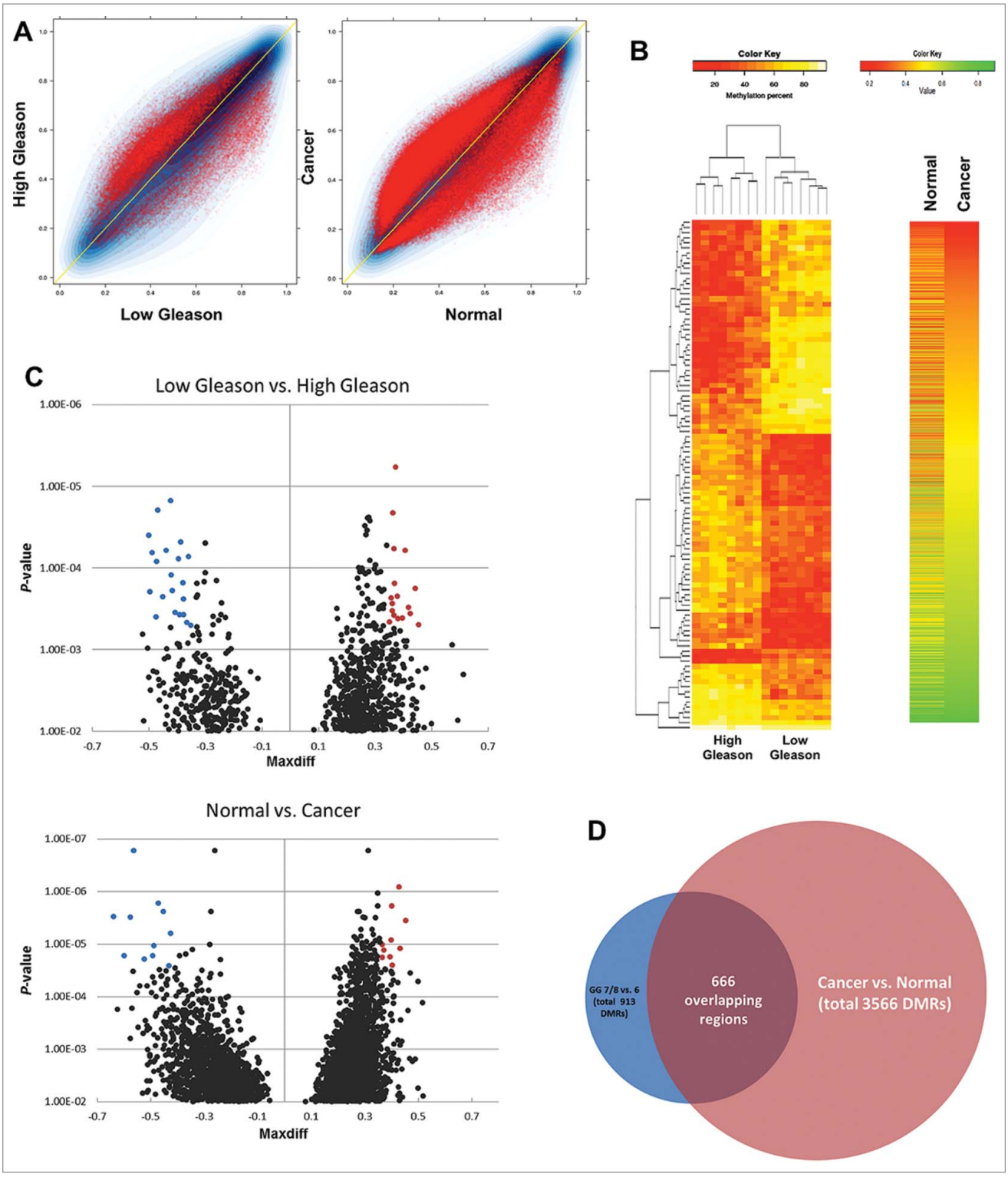

Figure 1. Global views of CHARM assay results. (A) Scatter plots show methylation values of individual probes in comparisons of low Gleason vs. high Gleason samples (left panel) and normal vs. cancer samples (right panel). Each point represents a probe from the CHARM assay. Highlighted in red is the subset of probes with significant differential methylation values, in positions used to group them into DMRs. The rest of the probes are shown in blue with the color scale representing density. (B) Heatmaps of DMRs comparing low Gleason vs. high Gleason (left panel) and normal vs. cancer (right panel). Each row represents a DMR. The left panel presents a hierarchical clustering of genome methylation values in 8 high-Gleason and 8 low-Gleason patient samples. The 100 CHARM probes in 913 DMRs with the largest magnitude t-statistic between the 2 groups were used; each column denotes a patient. The right panel presents group comparison between 10 normal individual and the same 16 prostate cancer patients as shown in the left panel. The rows are in ascending order according to the mean methylation of the DMR in the cancer group. (C) Volcano plot for CHARM analysis data sets. Each dot represents an individual DMR. The x-axis represents the difference of maximum methylation value (maxidiff) of DMRs between the comparisons. A positive maxidiff value indicates more methylation and a negative value indicates less methylation in high Gleason (upper panel) and cancer samples (lower panel). The y-axis shows the *P*-value for the DMRs. The blue and red dots are the select top candidate DMRs according to the rank of both maxidiff values and nominal *P*-values subjected to further technical validation. (D) Venn diagram showing the number of significant DMRs identified in comparisons of low Gleason vs. high Gleason (blue) and normal vs. cancer samples (pink), and the number of overlapping DMR regions between the 2 comparisons.

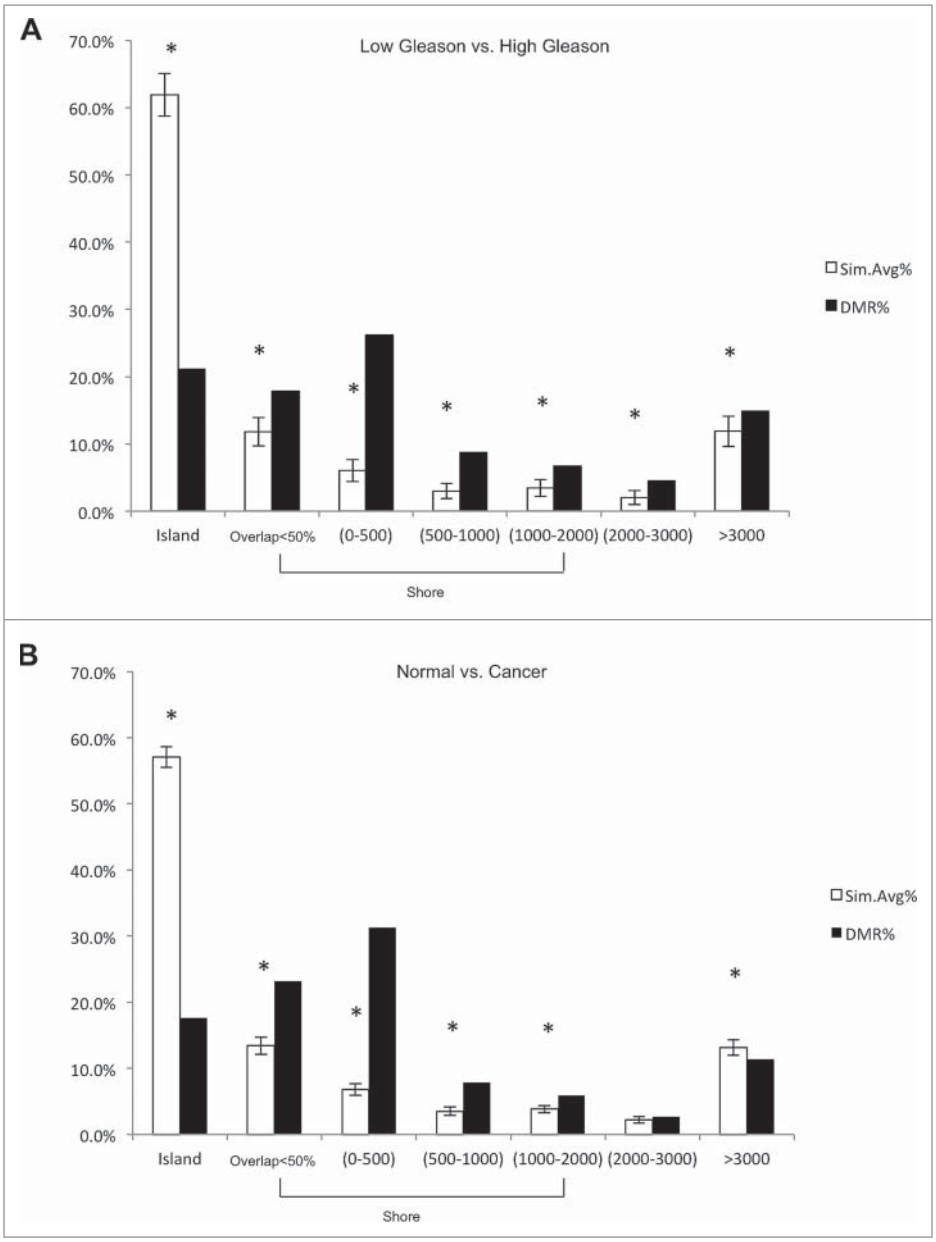

Figure 2. Distribution of DMRs of low Gleason vs. high Gleason (A) and normal vs. cancer (B) in the genome in relation to CpG islands (CGIs). As denoted on the X axis, DMR positions are defined as "Island" (cover or overlap with more than 50% of a CGI), "Shore" (including overlap with 0.1–50% of a CGI, or located 0-500, 500-1000, or 1000-2000 bp from the nearest CGI), 2000-3000 bp from the nearest CGI, or more than 3000 bp from the nearest CGI. The y-axis represents percentage of each group for the DMRs of interest. The white bars represent the simulated DMR distribution (the null hypothesis, mean±2xSD). The black bars represent the locations of CHARM assay identified DMRs. * $P<0.01$ for simulation vs. DMR distribution.

EXT1, IRX5, and *FLRT2* were also found to have significant differential methylation patterns (Fig. 3A-F). The directions of the methylation changes (hyper- or hypo-methylation) of these validated DMRs are all consistent with the CHARM results.

Among the previously reported genes differentially methylated based on Gleason score, *APC, PDLIM4, SFN*, and *SERPINB5* have been studied extensively in PCa.[12] Therefore, even though they were not among the top DMRs identified in our CHARM study, we included them for pyrosequencing analysis of the discovery cohort. Our results showed that *APC, PDLIM4*, and *SFN* were significantly hypermethylated in high-Gleason samples compared with low-Gleason samples (Fig. 3G-I).

To further investigate the correlation between the novel DMRs and progression of PCa, an additional 53 independent PCa samples, including 20 low-Gleason and 33 high-Gleason grade tissues, were used as a validation cohort to test the 9 DMRs. The results demonstrated that the methylation levels of *OPCML, FLRT2, SFN*, and *PDLIM4* differed significantly between low- and high-Gleason grade samples (Fig. 4A-D). *ELAVL2* and *EXT1* also showed a strong trend of differential methylation (Fig. 4E). Of the 4 DMRs with significant difference between low vs. high Gleason samples, *OPCML* and *PDLIM4* were the most informative per *P*-value. The combination of these 2 DMRs might be an effective diagnostic panel for future validation: the AUC from the combined ROC curve was 0.91 (Fig. 4F).

Table 2. Clinical pathological characteristics of the patients of outcome cohort.

	No recurrence N=86	Recurrence N=70
Gleason Score		
6 (3+3)	48	7
7 (3+4)	34	40
7 (4+3)	2	20
8-9	2	3
Age (y) at time of RRP		
mean ± SD	59±7	61±7
Range	47-78	43-76
Race		
Caucasian	69	56
Asian	2	0
Black	1	2
Hispanic	1	0
Indian (Native American)	1	0
Multi-Racial	12	11
Unknown	0	1
PSA at diagnosis, ng/ml		
≤10	71	52
>10	14	18
Unknown	1	0
mean ± SD	6.9±3.7	10.4±11.3
Pathological stage		
T2	72	47
T3	14	23
Surgical margin status		
Negative	73	35
Positive	13	33
Abuts	0	2
Perforated Capsule		
Negative	75	46
Positive	11	24
Post RRP recur		
Detectable Mets	0	10
Disease Free Interval	N/A	44±36

The impact of DMRs on biochemical recurrence

To further explore the prognostic value of the DMRs, we acquired a third cohort of patients with documented outcome data from the PCa repository (38 frozen tissues) and the Canary Foundation (133 FFPE tissues). Pyrosequencing of the 9 target DMRs was performed on all frozen and FFPE samples. Fifteen tumor specimens overlapped between the tissues acquired from the 2 specimen resources. The DMR methylation results for these 15 samples were compared. Fig. 5A shows *OPCML* DMR methylation in the 15 tumor samples demonstrating no significant difference between samples with different archiving method. We then combined the 2 sample sets as an outcome cohort. For the 15 overlapping samples, the pyrosequencing data from the Canary Foundation samples were used for analysis.

We first examined the methylation status of the *OPCML* DMR, comparing patients with biochemical recurrence vs. no recurrence. No difference was evident between these 2 groups (Fig. 5B). In addition, within the recurrence group, the *OPCML* DMR methylation levels were not associated with a disease-free interval based on Kaplan-Maier estimation (Fig. 5C). We then examined the methylation status of the *OPCML* DMR comparing low-Gleason and high-Gleason score groups within the outcome cohort; again, no significant difference was found (Fig. 5D). It should be noted that the majority of the GS 7 samples of the outcome cohort were GS 3+4 (74 cases), which constituted 77% of all 96 GS 7 samples, whereas the GS 7 samples

Table 3. The most relevant functional networks and biological processes present in the gene lists.

Low Gleason vs. high Gleason Top networks	Score
Embryonic Development, Nervous System Development and Function, organ Development	50
Skeletal and Muscular System Development and Function, Connective Tissue Development and Function, Embryonic Development	35
Cellular Development, Gene Expression, Embryonic Development	33
Organismal Injury and Abnormalities, Skeletal and Muscular Disorders, Neurological Disease	33
Cellular Development, Nervous System Development and Function, Visual System Development and Function	29
Top bio functions related to diseases and disorders	*P*-value
Developmental Disorder	5.11E-09 – 6.14E-04
Gastrointestinal Disease	5.11E-09 – 6.14E-04
Neurological Disease	4.09E-08 – 6.32E-04
Psychological Disorders	4.09E-08 – 4.47E-04
Skeletal and Muscular Disorders	1.39E-07 – 6.14E-04
Top canonical pathways	*P*-value
Basal Cell Carcinoma Signaling	5.57E-05
Corticotropin Releasing Hormone Signaling	9.83E-05
Neuropathic Pain Signaling In Dorsal Horn Neurons	8.48E-04
nNOS Signaling in Neurons	1.02E-03
Factors Promoting Cardiogenesis in Vertebrates	1.42E-03
Normal vs. Cancer Top networks	Score
RNA Post-Transcriptional Modification, Cell Cycle, Cellular Assembly and Organization	40
Nervous System Development and Function, Tissue Development, Tissue Morphology	38
Gene Expression, Cellular Development, Connective Tissue Development and Function	38
Cell Signaling, Carbohydrate Metabolism, Molecular Transport	38
Embryonic Development, Organismal Development, Skeletal and Muscular System Development and Function	36
Top bio functions related to diseases and disorders	*P*-value
Developmental Disorder	6.69E-18 – 3.69E-05
Skeletal and Muscular Disorders	3.60E-15 – 4.46E-05
Cancer	6.67E-15 – 4.25E-05
Gastrointestinal Disease	9.35E-14 – 1.69E-05
Neurological Disease	5.51E-11 – 4.46E-05
Top canonical pathways	*P*-value
EIF2 Signaling	1.16E-09
Transcriptional Regulatory Network in Embryonic Stem Cells	3.13E-08
Wnt/b-catenin Signaling	1.54E-05
Regulation of eIF4 and p70S6K Signaling	3.66E-05
Axonal Guidance Signaling	9.69E-05

in the discovery and validation cohorts were all (100%) GS 4+3 samples. It has been well established that GS 3+4 tumors have a better prognosis than GS 4+3 tumors,[13,14] and that Gleason 3+4 tumors have been suggested to be treated similarly to Gleason 6 tumors clinically. Our data indeed showed that the GS 3+4 cases behaved similarly to GS 6 and were significantly different from GS 4+3 (Fig. 5E, P=0.004). The number of GS 3+4 cases was roughly balanced in the recurrence

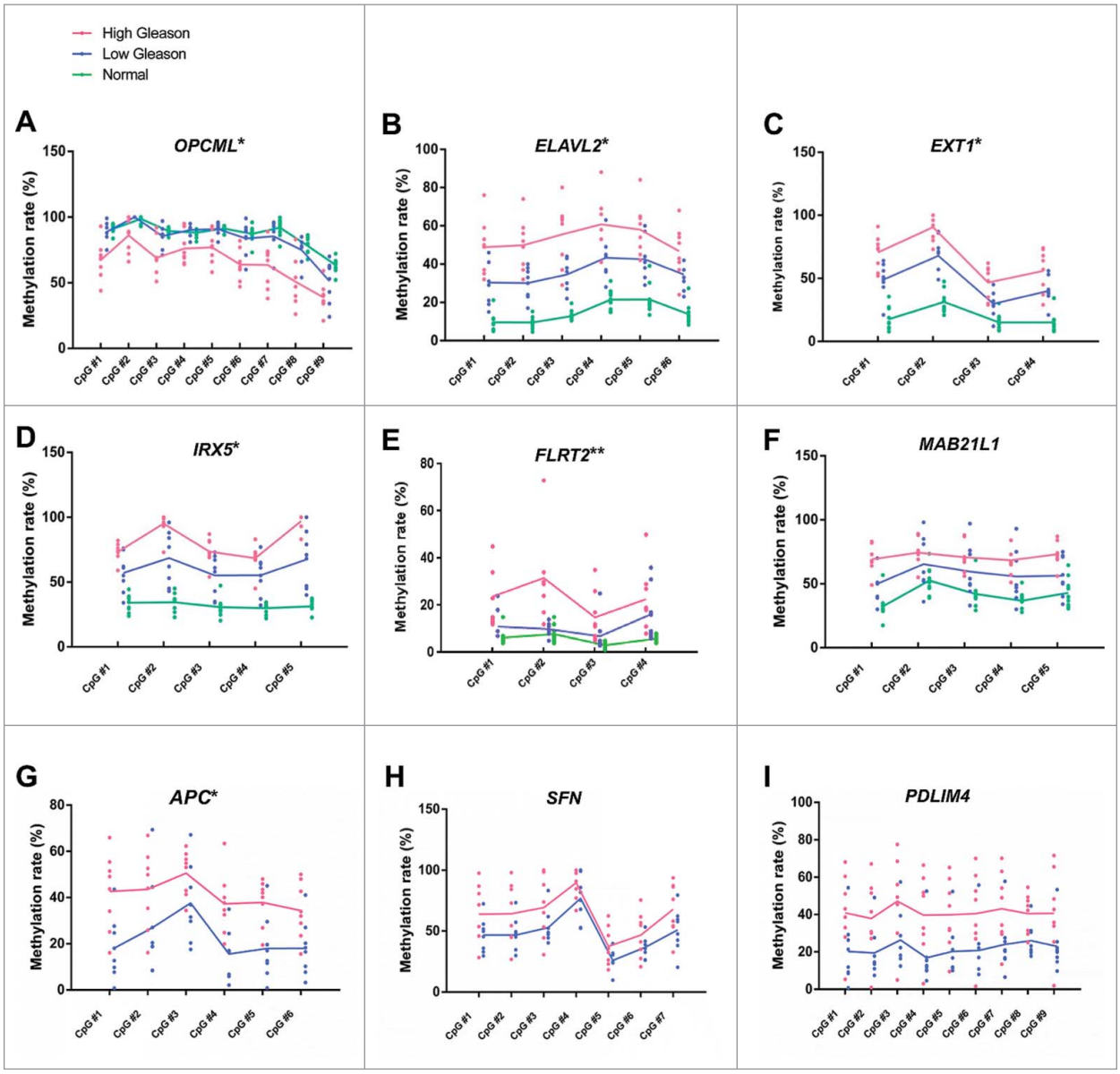

Figure 3. Bisulfite pyrosequencing analysis of 9 select DMRs using samples from the discovery cohort. Each dot represents methylation rate at the indicated CpG site of individual samples. The green, blue, and pink dots represent the normal, low-Gleason, and high-Gleason samples, respectively. The lines connect mean value of each CpG site within each group. Gene names are specified in each panel. * $P<0.01$ and ** $P<0.05$ for low-Gleason vs. high-Gleason tumors. Please note that the scales differ between the individual graphs.

(40 cases) and no recurrence (34 cases) groups. The methylation status of the *OPCML* DMR was not able to distinguish the 2 groups (Fig. 5F). When GS 3+4 cases were excluded, comparison of *OPCML* DMR methylation of the outcome cohort showed a small difference between the recurrence and no recurrence groups (Fig. 5G, $P=0.06$). Of course, because this subgroup analysis of GS 3+4 vs. GS 4+3 is post-hoc, it carries a high risk of yielding false positive results. The Kaplan-Maier curve for biochemical recurrence based on the Gleason sore is shown in Fig. 5H.

The cancer genome atlas (TCGA) database

To compare results with published high-throughput methylation studies and to use an external cohort as a validation dataset, we sought to mine the methylation data from the TCGA prostate adenocarcinoma (PRAD) database, which were generated by HumanMethylation450 BeadChip array (450K; Illumina, San Diego, CA). Data from the 450K array were informative for all 9 DMRs that we investigated. However, of the 160 tumors with Gleason score information recorded, only 11 cases of GS 6 and GS 8 had biochemical recurrence. We were therefore not able to perform statistical analysis with enough power to compare low GS vs. high GS or recurrence vs. no recurrence. In the PRAD cohort, the total 116 cases of GS 7 are comprised of 72 GS 3+4 and 44 GS 4+3 cases, but no significant difference of *OPCML* DMR methylation was found between these 2 subcategories (data not shown). RNA-seq data were also available for the 160 tumors, but no correlation was found between expression and methylation levels for either *OPCML* or *FLRT2* DMRs.

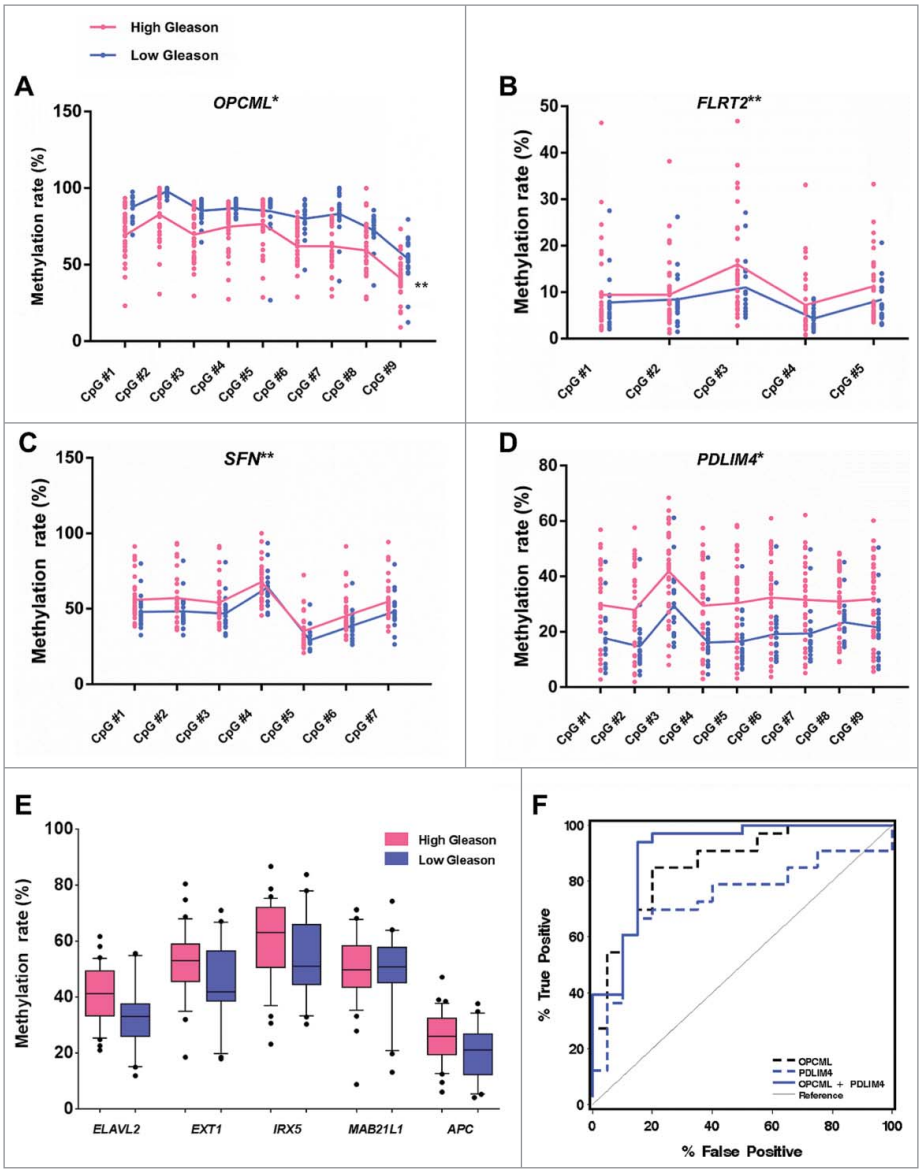

Figure 4. Bisulfite pyrosequencing analysis of 9 select DMRs using the validation cohort. Bisulfite pyrosequencing results are shown for (A) *OPCML;* (B) *FLRT2*; (C) *SFN*, and (D) *PDLIM4*. Each dot represents the percent of methylation of each sample at the indicated CpG site. The blue and pink dots represent the low Gleason and high Gleason samples, respectively. The lines connect mean value of each CpG site within each group. (E) Low-Gleason (blue) vs. high-Gleason (pink) bisulfite pyrosequencing results, shown as boxplots of mean values for *ELAVL2, EXT1, IRX5, MAB21L1*, and *APC*. Whiskers of the boxplots mark the 5th and 95th percentiles, the boxes mark the 25th percentile, median, and 75th percentile, while extreme values are shown as black dots. (F) Receiver operating characteristic (ROC) analysis of low-Gleason vs. high-Gleason using the validation cohort for prognostic potential of *OPCML*-DMR, *PDLIM4*-DMR, or the combination of the two. The area under the curve (AUC) is 0.86 for *OPCML*-DMR alone and 0.91 for the combination of *OPCML*-DMR and *PDLIM4*-DMR.

Integrative analysis of DMRs with copy number alterations

To evaluate whether the methylation of DMRs and the expression of DMR-related genes are correlated with genomic changes, we examined copy number alterations (CNAs) in all the discovery cohort samples except one low-GS case. Overall, larger numbers of CNAs were found in the high-Gleason group than in the low-Gleason group, including frequent loss of *PTEN, TMPRSS2*, and *ERG*, genes important in PCa.[15,16] There were also more DMRs and DMR-related genes affected by CNAs in the high-Gleason group (supplemental Fig. 2).

Discussion

With CHARM assay targeting genome-wide CpG sites to analyze differential DNA methylation comparing normal vs. PCa and low Gleason vs. high Gleason grade prostate tumors, we successfully identified series of DMRs in both comparisons. Most DMRs were found to be located in CGI shores instead of within CGIs, consistent with previous findings from other cancer types that show tissue-specific and tumor-specific DMRs are more concentrated in shore regions.[11,17] These results underscore the importance of methylation profiling through an unbiased, whole genome approach rather than the traditional approach that is focused on CGIs.

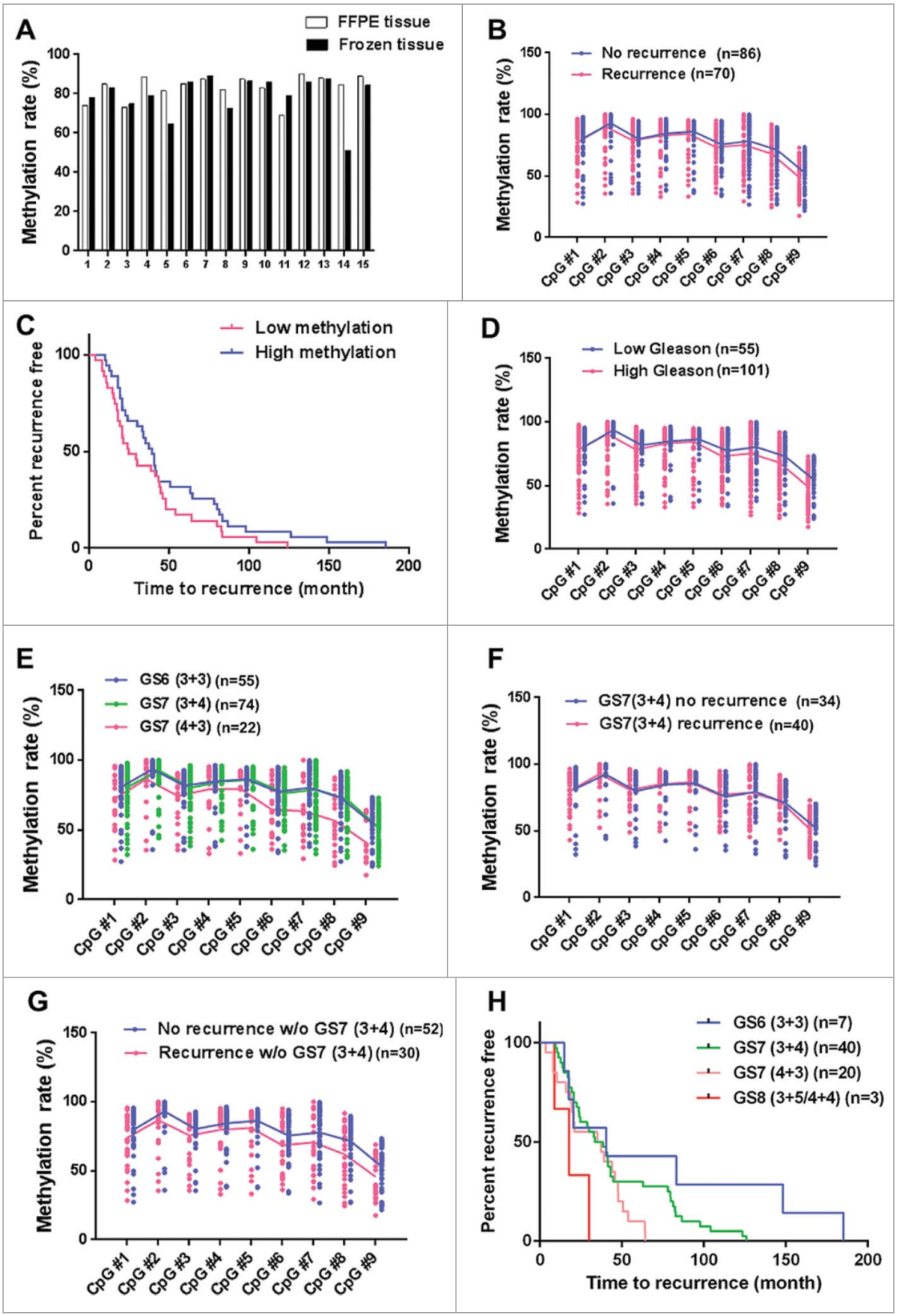

Figure 5. Bisulfite pyrosequencing analysis of *OPCML*-DMR using the outcome cohort. (A) Bisulfite pyrosequencing results of *OPCML*-DMR are shown for FFPE tissues (white bars) and frozen tissues (black bars) derived from the same patient tumor, total 15 tumors. For (B), (D), (E), (F), and (G), bisulfite pyrosequencing results are of *OPCML*-DMR in tumor samples of the outcome cohort. Each dot represents the percent of methylation at the indicated CpG site for each sample. The blue and pink dots represent the no recurrence and recurrence samples, respectively. The lines connect the mean values of each CpG site within each group. (C) Kaplan-Meier plot showing the relationship of methylation of *OPCML*-DMR and time to biochemical recurrence. Patients with biochemical recurrence were divided into a high- (blue) or low- (pink) *OPCML*-DMR methylation groups. Log-rank test P=0.52. (H) Kaplan-Meier plot showing the time to biochemical recurrence for patients based on Gleason scores in the outcome cohort (Table 2).

Of the DMRs identified from the comparison of low- vs. high-Gleason grade, 72.9% overlapped with 18.6% of total DMRs from the normal vs. cancer comparison. This suggests that, to a large extent, the same genomic regions acquired epigenetic changes in the transition from benign to cancerous prostate tissue as in disease progression from low- to high-Gleason grade. Our results also demonstrated higher frequency of hypermethylation in PCa in comparison with normal samples, supporting previous study results.[18] Furthermore, we found more frequent events of hypermethylation in high-Gleason tumors than in low-Gleason ones.

We identified novel candidate DMRs as candidate biomarkers to distinguish PCa vs. normal tissues, as well as low- vs. high-Gleason grade tumors. *OPCML* (opioid-binding cell adhesion molecule) is one of the top ranking DMRs that showed significant differential methylation patterns between high Gleason grade vs. low Gleason grade (high- vs. low-risk) groups in PCa. Interestingly, *OPCML* was originally reported to be epigenetically inactivated and have tumor-suppressor functions in epithelial ovarian cancer.[19] OPCML acts as a broad tumor suppressor for multiple carcinomas including PCa with frequent epigenetic inactivation.[20] In epithelial ovarian cancer, OPCML has been shown to negatively regulate a specific receptor tyrosine kinase (RTK) repertoire consisting of EPHA2, FGFR1, FGFR3, HER2, and HER4 receptors. OPCML functions through directly binding the extracellular domains of RTKs, shifting their trafficking pathways and downregulating RTK levels via polyubiquitination-associated proteasome degradation, eventually leading to signaling and growth inhibition.[21] The epigenetically inactivated region of *OPCML* reported by previous studies is located in the CGIs within the promoter region. In contrast, the *OPCML* DMR identified in our study is located in the CGI shore region. Considering that prostate and ovarian cancer are both sex-hormone regulated tumors and that OPCML exhibits interesting features of a tumor suppressor in multiple cancer types including prostate and ovarian, we hypothesize that the *OPCML*-DMR we identified may serve as an effective stratification marker for high- vs. low-risk PCa. Our finding of a predictive value of 0.89 based on AUC in distinguishing high- vs. low-Gleason tumors using *OPCML*-DMR alone (Fig. 4F) supports this hypothesis. However, our data has not shown prognostic value regarding biochemical recurrence using *OPCML*-DMR.

The other DMR validated in both the discovery and validation cohort is *FLRT2*. Together with 2 other factors, FLRT1 and FLRT3, the fibronectin leucine rich transmembrane proteins (FLRT) make a novel extracellular matrix protein family.[22] FLRT2 has been shown to function in cell adhesion and/or receptor signaling. Kunkel's group reported XFLRT3 and XFLRT2 as novel transmembrane modulators of fibroblast growth factor (FGF)–MAP kinase signaling.[23] Furthermore, FLRT2 was demonstrated to interact with fibroblast growth factor receptor 2 (FGFR2) in mouse embryonic craniofacial tissue lysates. Stable knockdown or overexpression of *FLRT2* in the chondrogenic cell line ATDC5 results in a corresponding decrease and increase of FGFR2 mRNA and protein expression, as well as downstream ERK phosphorylation levels.[24] FGF signaling regulates many important biological processes including cell proliferation, differentiation, and migration during development.[25] The human *FGFR2* gene encodes FGFR2b and FGFR2c isoforms,[26-29] The hallmark of tumor invasion and metastasis, epithelial-to-mesenchymal transition (EMT) is accompanied by a switch from exclusive expression of FGFR2b to FGFR2c in the rat PCa model.[30] Moreover, restoration of FGFR2b led to suppression of PC-3 cell growth *in vitro* as well as reduced tumor formation *in vivo*.[31] Therefore, FGFR2b is considered a tumor-suppressor in PCa. To date, there has been no report indicating FLRT2 is directly related to PCa; however, several papers implicate that FGFR2 might bridge the gap. Therefore, given the fact that human and mouse FLRT2 share 97% homology at protein level,[32] and FGFR2b is interacting with and regulated by FLRT2 in mice and could potentially be anti-oncogenic in PCa, we hypothesize that the differential methylation of the region encompassing the *FLRT2* transcription start site (TSS) might play a novel role in regulating the expression and interaction of FLRT2 and FGFR2, thereby modulating PCa progression.

Other novel DMRs identified in the discovery cohort, namely *ELAVL2, EXT1, IRX5*, and *MAB21L1*, all showed elevated methylation in high Gleason score tumors. *ELAVL2* (embryonic lethal abnormal vision-like 2) encodes a highly conserved, neural-specific RNA-binding protein.[33] EXT1 (Exostoses-1) is a reported tumor suppressor in mice. Hypermethylation of the *EXT1* CGI promoter led to transcriptional silencing of the *EXT1* gene and subsequent loss of heparin sulfate.[34] *EXT1* expression was significantly lower in benign prostatic hyperplasia (BPH) and PCa in comparison with normal prostate tissue.[35] IRX5 has been linked to human PCa through downregulation via vitamin D3 [1,25(OH)2D3] in LNCaP cells; VitD3 is a potent inhibitor of the proliferation of many different cancer cell types. Knockdown of *IRX5* resulted in an increase in p21 protein expression, G2-M arrest, and apoptosis, partially mediated by p53.[36] The *MAB21L1* gene has a highly polymorphic tandem CAG trinucleotide repeat in the 5′ UTR potentially associated with neurologic and psychiatric disorders.[37-39] Further studies are needed to explore the biological functions of the methylation status of these DMRs in PCa. The changes in the expression of these genes in prostate cancer, both the prevalence and extent, remain to be ascertained.

In this study we also included 3 well-studied DMRs: *APC, PDLIM4*, and *SFN*. These were all reported to be associated with the Gleason score in PCa;[12] however, we were not able to validate them as consistent DMRs in all of our cohorts. Our results showed significant differential methylation of *APC* in the discovery cohort but not in the validation cohort and, alternatively, differential methylation of *PDLIM4* and *SFN* in the validation cohort but not in the discovery cohort. None of these 3 genes showed differential methylation patterns in the comparison of tumor samples with or without biochemical recurrence. Assays based on patient tissues are limited by the impact of infection/inflammation, which may partially explain the lack of significance of these markers in our cohort. For example, *APC* methylation is associated with inflammation.[40] We do not have information regarding inflammation in these samples. Age may also complicate the results as DNA methylation changes with aging.

Even though CHARM is a robust and non-biased method to assess the methylation of CpG sites throughout the whole

genome, it requires large amount of input DNA (5 μg). This limits the sample availability for the CHARM assay in this study. Another limitation of the study is the sample size of our validation and outcome cohorts. Additional samples with complete clinical information are critical to validate our novel DMRs in order to determine the clinical utility of these markers. A recent European study on over 400 total samples reported 6 novel candidate DNA methylation markers for PCa; 3 of these markers, *C1orf114, AOX1*, and *HAPLN3*, were independent predictors of time to biochemical recurrence after radical prostatectomy.[41] Additional emerging candidate markers for prognosis were also published.[42,43] Cross validation of these potential prognostic markers in various cohorts will be important to confirm truly useful methylation markers for clinical practice.

In summary, whole-genome methylation profiling with CHARM revealed distinct patterns of differential DNA methylation between normal prostate and PCa tissues, as well as between different risk groups of PCas defined by Gleason scores. We identified several novel DMRs including *OPCML, ELAVL2, EXT1, FLRT2*, and *IRX5* to effectively distinguish low- from high-Gleason grade PCas. In particular, *OPCML* and *FLRT2* were further validated in independent cohorts. However, these DMRs showed no significant difference of methylation in patients with or without biochemical recurrence. Further investigation is needed to validate the prognostic value of the novel DMRs and to explore the biological functions of their differentially methylated status in PCa.

Patients and materials/methods

This study was approved by the Institutional Review Boards (IRB) of the Fred Hutchinson Cancer Research Center and the University of Washington.

Study subjects

All tissue specimens in this study were obtained from the PCa repository, University of Washington (PI: Robert Vessella) and Canary Foundation (PtdIns: Pete Nelson). The tumor cell content of all the cancer specimens was 75% or higher. The discovery cohort included fresh frozen PCa tissues (n=16) and matched normal prostate tissues (n=10) from a total of 16 age-matched PCa patients. The validation cohort included 53 fresh frozen PCa tissues. The clinical pathological characteristics of the patients in the discovery and validation cohorts are shown in Table 1. The outcome cohort initially included 38 frozen tissues (from PCa repository, UW) and 133 FFPE tissues (from Canary Foundation). Fifteen tumor samples overlapped between the tissues acquired from the 2 specimen resources. Based on comparable results, we combined the 2 sample sets to form the outcome cohort and used the pyrosequencing results from the FFPE tissue for further analysis of the overlapped samples. Therefore, the outcome cohort included a total of 156 samples. Of these, 86 had no biochemical recurrence and 70 did. The clinical pathological characteristics of the patients of the outcome cohort are shown in Table 2. Gleason scores were previously reviewed by a pathologist.

DNA extractions

Genomic DNA of frozen tissue was isolated using Gentra Puregene Kit (Qiagen, cat. no. 158667). Genomic DNA of FFPE tissue was isolated using QiAamp DSP DNA FFPE tissue kit (Qiagen, cat. no. 60404) per user manual for CytoScan DNA purification from FFPE tissue (Affymetrix, cat. no. 901835).

CHARM microarray

CHARM microarrays were performed as previously described.[44] Briefly, 5 μg of DNA from each specimen was randomly fractionated with HydroShear, divided into 2 equal portions to be treated with and without McrBC, a restriction enzyme that cleaves DNA containing 5-methylcytosine preceded by a purine nucleotide, then size fractionated by agarose gel electrophoresis, purified and subjected to whole-genome amplification prior to hybridization with the CHARM array (customized NimbleGen HD2 array, Roche, cat. no. B7074-00-01). The raw data were analyzed with the R/Bioconductor CHARM package (Analysis of DNA methylation data from CHARM microarrays, http://bioconductor.org/packages/release/bioc/html/charm.html). Differential methylation was quantified for each pairwise tissue comparison by the difference of averaged and normalized methylation values (ΔM). Z scores were calculated using ΔM and standard errors (s.e.m) {z = [ΔM /s.e.m. (ΔM)]}. Probes carrying z scores with a false discovery rate (FDR) $\leq$5 % and contiguous in positions were grouped into DMRs. DMRs with *P*-values lower than 0.01 in permutation test were considered statistically significant.

Bisulfite conversion and pyrosequencing

DNA (100 ng) was used for bisulfite conversion, which was performed using EpiTect Bisulfite Kit (Qiagen, cat. no. 59104) or EZ-96 DNA Methylation-Direc Kit (Zymo Research, cat. no. D5022), according to the manufacturers' protocols. Primer sets with one biotin-labeled primer for the amplification of the bisulfite-converted DNA were either from a pre-designed PyroMark CpG assay (Qiagen, 978746) or custom designed using PyroMark Assay Design software version 2.0.1.15 (Qiagen, cat. no. 9019077). PCR reactions were performed using PyroMark PCR kit (Qiagen, cat. no. 978703) according to the manufacturer's protocol. The pyrosequencing analysis was carried out using PyroMark Q24 or MD96 Systems (Qiagen, cat. no. 9001514) to assess the quantitative methylation of the target genomic regions (Supplemental Table 1).

Integrative functional analysis

The analysis of the most relevant functional networks and biological processes present in the gene lists was generated through the use of IPA (Ingenuity Systems).

Chromosomal genomic array testing (CGAT)

Genomic DNA was tested on either CytoScanHD or SNP6.0 (Affymetrix, cat. no. 901835 and 901153, respectively), as per manufacturer's protocols. Copy number alteration and loss of

heterozygosity were assessed using an algorithm established at the Seattle Cancer Care Alliance based on the Hidden Markov model. Data analysis and visualization was performed with Nexus software (BioDiscovery).

Statistical analysis

The significance of differences between the null hypothesis and DMR distribution in Fig. 2 was determined by the X^2 test. For analysis of pyrosequencing results, since methylation levels exhibited parallel profiles across CpG sites within a given DMR, statistical comparisons of methylation were based on the average methylation level across CpG sites. Comparisons between groups were by 2-sample t-test. Linear regression was used to adjust for age and other clinical factors. Logistic regression was used to evaluate area under the receiver operating characteristic (ROC) curve, to assess the ability of single or multiple DMRs to distinguish PCa with high vs. low Gleason grade.

Disclosure of potential conflicts of interest

No potential conflicts of interest were disclosed.

Funding

This study was supported by P01 Pacific NW SPORE and SUB CA085859 awarded by the National Cancer Institute.

References

1. Mackinnon AC, Yan BC, Joseph LJ, Al-Ahmadie HA. Molecular biology underlying the clinical heterogeneity of prostate cancer: an update. Arch Pathol Lab Med 2009; 133:1033-40; PMID:19642730
2. Michaelson MD, Cotter SE, Gargollo PC, Zietman AL, Dahl DM, Smith MR. Management of complications of prostate cancer treatment. CA Cancer J Clin 2008; 58:196-213; PMID:18502900; http://dx.doi.org/10.3322/CA.2008.0002
3. Nelson WG, De Marzo AM, Yegnasubramanian S. Epigenetic alterations in human prostate cancers. Endocrinology 2009; 150:3991-4002; PMID:19520778; http://dx.doi.org/10.1210/en.2009-0573
4. Cooper CS, Foster CS. Concepts of epigenetics in prostate cancer development. Br J Cancer 2009; 100:240-5; PMID:19002169; http://dx.doi.org/10.1038/sj.bjc.6604771
5. Yegnasubramanian S, Haffner MC, Zhang Y, Gurel B, Cornish TC, Wu Z, Irizarry RA, Morgan J, Hicks J, DeWeese TL, et al. DNA hypomethylation arises later in prostate cancer progression than CpG island hypermethylation and contributes to metastatic tumor heterogeneity. Cancer Res 2008; 68:8954-67; PMID:18974140; http://dx.doi.org/10.1158/0008-5472.CAN-07-6088
6. Schoenborn JR, Nelson P, Fang M. Genomic profiling defines subtypes of prostate cancer with the potential for therapeutic stratification. Clin Cancer Res 2013; 19:4058-66; PMID:23704282; http://dx.doi.org/10.1158/1078-0432.CCR-12-3606
7. Chao C, Chi M, Preciado M, Black MH. Methylation markers for prostate cancer prognosis: a systematic review. Cancer Causes Control 2013; 24:1615-41; PMID:23797237; http://dx.doi.org/10.1007/s10552-013-0249-2
8. Goering W, Kloth M, Schulz WA. DNA methylation changes in prostate cancer. Methods Mol Biol 2012; 863:47-66; PMID:22359287; http://dx.doi.org/10.1007/978-1-61779-612-8_4
9. Chiam K, Ricciardelli C, Bianco-Miotto T. Epigenetic biomarkers in prostate cancer: Current and future uses. Cancer Lett 2014; 342:248-56; PMID:22391123; http://dx.doi.org/10.1016/j.canlet.2012.02.011
10. Doi A, Park IH, Wen B, Murakami P, Aryee MJ, Irizarry R, Herb B, Ladd-Acosta C, Rho J, Loewer S, et al. Differential methylation of tissue- and cancer-specific CpG island shores distinguishes human induced pluripotent stem cells, embryonic stem cells and fibroblasts. Nat Genet 2009; 41:1350-3; PMID:19881528; http://dx.doi.org/10.1038/ng.471
11. Irizarry RA, Ladd-Acosta C, Wen B, Wu Z, Montano C, Onyango P, Cui H, Gabo K, Rongione M, Webster M, et al. The human colon cancer methylome shows similar hypo- and hypermethylation at conserved tissue-specific CpG island shores. Nat Genet 2009; 41:178-86; PMID:19151715; http://dx.doi.org/10.1038/ng.298
12. Vasiljevic N, Wu K, Brentnall AR, Kim DC, Thorat MA, Kudahetti SC, Mao X, Xue L, Yu Y, Shaw GL, et al. Absolute quantitation of DNA methylation of 28 candidate genes in prostate cancer using pyrosequencing. Dis Markers 2011; 30:151-61; PMID:21694441; http://dx.doi.org/10.1155/2011/157829
13. Stephenson AJ, Kattan MW. Nomograms for prostate cancer. BJU Int 2006; 98:39-46; PMID:16831140; http://dx.doi.org/10.1111/j.1464-410X.2006.06173.x
14. Stark JR, Perner S, Stampfer MJ, Sinnott JA, Finn S, Eisenstein AS, Ma J, Fiorentino M, Kurth T, Loda M, et al. Gleason score and lethal prostate cancer: does 3 + 4 = 4 + 3? J Clin Oncol 2009; 27:3459-64; PMID:19433685; http://dx.doi.org/10.1200/JCO.2008.20.4669
15. Qu X, Randhawa G, Friedman C, Kurland BF, Glaskova L, Coleman I, Mostaghel E, Higano CS, Porter C, Vessella R, et al. A three-marker FISH panel detects more genetic aberrations of AR, PTEN and TMPRSS2/ERG in castration-resistant or metastatic prostate cancers than in primary prostate tumors. PLoS One 2013; 8:e74671; PMID:24098661; http://dx.doi.org/10.1371/journal.pone.0074671
16. Qu X, Randhawa G, Friedman C, O'Hara-Larrivee S, Kroeger K, Dumpit R, True L, Vakar-Lopez F, Porter C, Vessella R, et al. A novel four-color fluorescence in situ hybridization assay for the detection of TMPRSS2 and ERG rearrangements in prostate cancer. Cancer Genet 2013; 206:1-11; PMID:23352841; http://dx.doi.org/10.1016/j.cancergen.2012.12.004
17. Irizarry RA, Ladd-Acosta C, Carvalho B, Wu H, Brandenburg SA, Jeddeloh JA, Wen B, Feinberg AP. Comprehensive high-throughput arrays for relative methylation (CHARM). Genome Res 2008; 18:780-90; PMID:18316654; http://dx.doi.org/10.1101/gr.7301508
18. Devaney JM, Wang S, Funda S, Long J, Taghipour DJ, Tbaishat R, Furbert-Harris P, Ittmann M, Kwabi-Addo B. Identification of novel DNA-methylated genes that correlate with human prostate cancer and high-grade prostatic intraepithelial neoplasia. Prostate Cancer Prostatic Dis 2013; 16:292-300; PMID:23896626; http://dx.doi.org/10.1038/pcan.2013.21
19. Sellar GC, Watt KP, Rabiasz GJ, Stronach EA, Li L, Miller EP, Massie CE, Miller J, Contreras-Moreira B, Scott D, et al. OPCML at 11q25 is epigenetically inactivated and has tumor-suppressor function in epithelial ovarian cancer. Nat Genet 2003; 34:337-43; PMID:12819783; http://dx.doi.org/10.1038/ng1183
20. Cui Y, Ying Y, van Hasselt A, Ng KM, Yu J, Zhang Q, Jin J, Liu D, Rhim JS, Rha SY, et al. OPCML is a broad tumor suppressor for multiple carcinomas and lymphomas with frequently epigenetic inactivation. PLoS One 2008; 3:e2990; PMID:18714356; http://dx.doi.org/10.1371/journal.pone.0002990
21. McKie AB, Vaughan S, Zanini E, Okon IS, Louis L, de Sousa C, Greene MI, Wang Q, Agarwal R, Shaposhnikov D, et al. The OPCML tumor suppressor functions as a cell surface repressor-adaptor, negatively regulating receptor tyrosine kinases in epithelial ovarian cancer. Cancer Discov 2012; 2:156-71; PMID:22585860; http://dx.doi.org/10.1158/2159-8290.CD-11-0256
22. Lacy SE, Bonnemann CG, Buzney EA, Kunkel LM. Identification of FLRT1, FLRT2, and FLRT3: a novel family of transmembrane leucine-rich repeat proteins. Genomics 1999; 62:417-26; PMID:10644439; http://dx.doi.org/10.1006/geno.1999.6033
23. Bottcher RT, Pollet N, Delius H, Niehrs C. The transmembrane protein XFLRT3 forms a complex with FGF receptors and promotes FGF signalling. Nat Cell Biol 2004; 6:38-44; PMID:14688794; http://dx.doi.org/10.1038/ncb1082

24. Wei K, Xu Y, Tse H, Manolson MF, Gong SG. Mouse FLRT2 interacts with the extracellular and intracellular regions of FGFR2. J Dent Res 2011; 90:1234-9; PMID:21765038; http://dx.doi.org/10.1177/0022034511415272
25. Lanner F, Rossant J. The role of FGF/Erk signaling in pluripotent cells. Development 2010; 137:3351-60; PMID:20876656; http://dx.doi.org/10.1242/dev.050146
26. Dionne CA, Crumley G, Bellot F, Kaplow JM, Searfoss G, Ruta M, Burgess WH, Jaye M, Schlessinger J. Cloning and expression of two distinct high-affinity receptors cross-reacting with acidic and basic fibroblast growth factors. EMBO J 1990; 9:2685-92; PMID:1697263
27. Miki T, Fleming TP, Bottaro DP, Rubin JS, Ron D, Aaronson SA. Expression cDNA cloning of the KGF receptor by creation of a transforming autocrine loop. Science 1991; 251:72-5; PMID:1846048; http://dx.doi.org/10.1126/science.1846048
28. Carstens RP, Wagner EJ, Garcia-Blanco MA. An intronic splicing silencer causes skipping of the IIIb exon of fibroblast growth factor receptor 2 through involvement of polypyrimidine tract binding protein. Mol Cell Biol 2000; 20:7388-400; PMID:10982855; http://dx.doi.org/10.1128/MCB.20.19.7388-7400.2000
29. Katoh M, Katoh M. FGFR2 and WDR11 are neighboring oncogene and tumor suppressor gene on human chromosome 10q26. Int J Oncol 2003; 22:1155-9; PMID:12684685; http://dx.doi.org/10.3892/ijo.22.5.1155
30. Yan G, Fukabori Y, McBride G, Nikolaropolous S, McKeehan WL. Exon switching and activation of stromal and embryonic fibroblast growth factor (FGF)-FGF receptor genes in prostate epithelial cells accompany stromal independence and malignancy. Mol Cell Biol 1993; 13:4513-22; PMID:7687739; http://dx.doi.org/10.1128/MCB.13.8.4513
31. Yasumoto H, Matsubara A, Mutaguchi K, Usui T, McKeehan WL. Restoration of fibroblast growth factor receptor2 suppresses growth and tumorigenicity of malignant human prostate carcinoma PC-3 cells. Prostate 2004; 61:236-42; PMID:15368475; http://dx.doi.org/10.1002/pros.20093
32. Haines BP, Wheldon LM, Summerbell D, Heath JK, Rigby PW. Regulated expression of FLRT genes implies a functional role in the regulation of FGF signalling during mouse development. Dev Biol 2006; 297:14-25; PMID:16872596; http://dx.doi.org/10.1016/j.ydbio.2006.04.004
33. King PH. Hel-N2: a novel isoform of Hel-N1 which is conserved in rat neural tissue and produced in early embryogenesis. Gene 1994; 151:261-5; PMID:7828887; http://dx.doi.org/10.1016/0378-1119(94)90668-8
34. Ropero S, Setien F, Espada J, Fraga MF, Herranz M, Asp J, Benassi MS, Franchi A, Patino A, Ward LS, et al. Epigenetic loss of the familial tumor-suppressor gene exostosin-1 (EXT1) disrupts heparan sulfate synthesis in cancer cells. Hum Mol Genet 2004; 13:2753-65; PMID:15385438; http://dx.doi.org/10.1093/hmg/ddh298
35. Suhovskih AV, Tsidulko AY, Kutsenko OS, Kovner AV, Aidagulova SV, Ernberg I, Grigorieva EV. Transcriptional Activity of Heparan Sulfate Biosynthetic Machinery is Specifically Impaired in Benign Prostate Hyperplasia and Prostate Cancer. Front Oncol 2014; 4:79; PMID:24782989; http://dx.doi.org/10.3389/fonc.2014.00079
36. Myrthue A, Rademacher BL, Pittsenbarger J, Kutyba-Brooks B, Gantner M, Qian DZ, Beer TM. The iroquois homeobox gene 5 is regulated by 1,25-dihydroxyvitamin D3 in human prostate cancer and regulates apoptosis and the cell cycle in LNCaP prostate cancer cells. Clin Cancer Res 2008; 14:3562-70; PMID:18519790; http://dx.doi.org/10.1158/1078-0432.CCR-07-4649
37. Margolis RL, Stine OC, McInnis MG, Ranen NG, Rubinsztein DC, Leggo J, Brando LV, Kidwai AS, Loev SJ, Breschel TS, et al. cDNA cloning of a human homologue of the Caenorhabditis elegans cell fate-determining gene mab-21: expression, chromosomal localization and analysis of a highly polymorphic (CAG)n trinucleotide repeat. Hum Mol Genet 1996; 5:607-16; PMID:8733127; http://dx.doi.org/10.1093/hmg/5.5.607
38. Margolis RL, Stine OC, Ward CM, Franz ML, Rosenblatt A, Callahan C, Sherr M, Ross CA, Potter NT. Unstable expansion of the CAG trinucleotide repeat in MAB21L1: report of a second pedigree and effect on protein expression. J Med Genet 1999; 36:62-4; PMID:9950369
39. Potter NT. Meiotic instability associated with the CAGR1 trinucleotide repeat at 13q13. J Med Genet 1997; 34:411-3; PMID:9152839; http://dx.doi.org/10.1136/jmg.34.5.411
40. Van der Auwera I, Van Laere SJ, Van den Bosch SM, Van den Eynden GG, Trinh BX, van Dam PA, Colpaert CG, van Engeland M, Van Marck EA, Vermeulen PB, et al. Aberrant methylation of the Adenomatous Polyposis Coli (APC) gene promoter is associated with the inflammatory breast cancer phenotype. Br J Cancer 2008; 99:1735-42; PMID:18841156; http://dx.doi.org/10.1038/sj.bjc.6604705
41. Haldrup C, Mundbjerg K, Vestergaard EM, Lamy P, Wild P, Schulz WA, Arsov C, Visakorpi T, Borre M, Hoyer S, et al. DNA methylation signatures for prediction of biochemical recurrence after radical prostatectomy of clinically localized prostate cancer. J Clin Oncol 2013; 31:3250-8; PMID:23918943; http://dx.doi.org/10.1200/JCO.2012.47.1847
42. Strand SH, Orntoft TF, Sorensen KD. Prognostic DNA methylation markers for prostate cancer. Int J Mol Sci 2014; 15:16544-76; PMID:25238417; http://dx.doi.org/10.3390/ijms150916544
43. Blute ML, Jr., Damaschke NA, Jarrard DF. The epigenetics of prostate cancer diagnosis and prognosis: update on clinical applications. Curr Opin Urol 2015; 25:83-8; PMID:25405932; http://dx.doi.org/10.1097/MOU.0000000000000132
44. Ladd-Acosta C, Aryee MJ, Ordway JM, Feinberg AP. Comprehensive high-throughput arrays for relative methylation (CHARM). Curr Protoc Hum Genet 2010; Chapter 20:Unit 20 1:1-19; PMID:20891028; http://dx.doi.org/10.1002/0471142905.hg2001s65